J Inorg Organomet Polym (2017) 27:1466–1472
DOI 10.1007/s10904-017-0604-y

Preparation by Sol–Gel Method and Characterization of Co-doped $LaNiO_3$ Perovskite

Elies Omari[1] · Sofiane Makhloufi[1] · Mahmoud Omari[1]

Received: 9 April 2017 / Accepted: 19 June 2017 / Published online: 22 June 2017

Abstract The effect of partial substitution of nickel by cobalt in perovskite $LaNi_{1-x}Co_xO_3$ $(0 \le x \le 0.6)$ oxides, synthesized by the sol–gel method, using nickel and/or cobalt nitrates, lanthanum nitrate, citric acid as chelating agent has been studied. The obtained samples were characterized by several techniques. XRD and IR analysis show that the formation of the perovskite phase occurs at 750 °C. Scanning electron microscopy (SEM) revealed that powders were composed of particles with different shape and size. The increase in the fraction of the doped-Co leads to highly agglomeration of particles while the porosity decreases. The electrochemical measurements shows that the presence of cobalt leads to a decrease of the catalytic activity attributed to the Co–Ni alloy formation. The highest electrode performance is achieved with $LaNi_{0.6}Co_{0.4}O_3$ electrode. The band gap energy was calculated from the UV–Visible and it is found above 3 eV.

Keywords $LaNi_{1-x}Co_xO_3$ · Perovskite · Sol–gel · Thermal analysis · Electrochemical properties · Optical properties

1 Introduction

The Perovskite-type mixed oxides are ceramic materials that combine metals elements with non-metallic ones usually can be described by the general stoichiometric formula ABO_3, where A represents a lanthanide or alkaline earth ion and B a trivalent ion of a transition metal. The perovskite lattice can accommodate multiple cationic substitutions with only small changes since the values of the structure factors (t) is between 0.75 and 1 [1]. In this structure, the properties are mainly determined by the occupancy of B sites, which usually are partially substituted [1, 2]. During these last years, theoretical and technological studies for mixed oxides with perovskite structure have developed based on their physical (ferroelectric, piezoelectric, magnetic, electro-optic, dielectric, conducting and superconducting properties and catalytic properties) [3–5]. The perovskite type catalysts containing nickel, such as $LaNiO_3$ have received much attention because of their potential application as electrode materials in solid oxide fuel cells, gas sensors. They have a structure relatively stable when heated and a good activity for the steam reforming which produces CO_2 and H_2O under oxidative conditions [6, 7]. The effect of the routes of preparation and calcination (temperature, time and atmosphere) and substitutions of A and/or B sites on the phase composition and crystalline structure of $LaNiO_3$ materials are considered important because of their effects on the electronic properties, which affect the conductivity and catalytic properties of the final product [8–11].

There are several chemical methods which can be used to synthesize metal oxide nanoparticles. Among these preparation methods, the sol–gel synthesis method has several advantages over other methods including good homogeneity, low cost, high purity and low heat treatment [12–14].

$LaNiO_3$ oxide has been much studied by doping of a nickelate site for practical applications. It was found that catalytic activities of $LaNi_{1-x}M_xO_3$ (M = Mn, Al, Co) complex oxides were much higher than that of $LaFeO_3$ sample due to the increase of the valence of B-site cations and lattice oxygen content [15]. In recent years, some research on

✉ Mahmoud Omari
m.omari@univ-biskra.dz

[1] Laboratory of Molecular Chemistry and Environment, University of Biskra, B. P. 145, 07000 Biskra, Algeria

the $LaNi_{1-x}Co_xO_3$ system was conducted. Valderrama et al. [16] have prepared $LaNi_{1-x}Co_xO_3$ ($0 \le x \le 1$) oxides by calcining the precursors at 750 °C for 4 h using the propionic acid as the solvent via a sol–gel resin method, used them as catalysts in the drying reforming of methane. Moreover, Androulakis et al. [17] have studied the electrical resistivity and the magneto-resistance of the metallic members of the $LaNi_{1-x}Co_xO_3$ series with $0.3 \le x \le 0.6$, synthesized via Pechini (citrate–gel) method. Some years later, Silva et al. [18] have synthesized a series of $LaNi_{1-x}Co_xO_3$ compounds ($x = 0$, 0.2 and 0.4) by the combustion method and used them as catalysts precursors in the partial oxidation of methane (POM). Recently, Zhong et al. [19] have prepared the series oxides of $LaNi_{1-x}Co_xO_3$ ($x = 0$, 0.1, 0.3, 0.7, 1.0) by a co-precipitation method, investigated the catalytic oxidation of NO. Furthermore, Zhao et al. [20] have reported the catalytic properties for steam reforming of ethanol using $LaNi_{1-x}Co_xO_3$ as catalysts obtained by calcining the precursors at 700 °C for 5 h via one step-citrate complexing method.

To our best knowledge, there is no works in the literature on the thermal stability, oxygen evolution reaction in alkaline media and optical properties of $LaNi_{1-x}Co_xO_3$ oxides.

In this present work, we started ours investigations on $LaNi_{1-x}Co_xO_3$ ($0 \le x \le 0.6$) oxides by the thermal evolution of the precursor powder prepared via sol–gel method, to the point of the formation of the perovskite phase, followed by means of thermal analysis, IR spectroscopy and powder X-ray diffraction (XRD). Thereafter, electrochemical measurements were performed with cyclic voltammetry at a scan rate of 20 mV/s in the potential range 0–0.8 V, aiming to determine the best material composition for the oxygen evolution reaction. Finally, optical band gap values were estimated using UV–Visible spectroscopy to measure the potential of our materials to be used as photo-catalysts.

2 Experimental Method

2.1 Preparation

$LaNi_{1-x}Co_xO_3$ ($0 \le x \le 0.6$) perovskites were synthesized by sol–gel method using lanthanum, nickel and cobalt nitrates as starting materials and citric acid as a complexing agent. Precursor solutions were prepared from stoichiometric amounts of precursor salts $La(NO_3)_3{\cdot}6H_2O$ (biochem), $Ni(NO_3)_2{\cdot}6H_2O$ (biochem), and $Co(NO_3)_2{\cdot}6H_2O$ (biochem) and along with citric acid were dissolved in ethanol. The solution with metal ions and citric acid in the molar ration 1:1:2 (lanthanum–nickel, cobalt–citric acid) are heated at 60–70 °C for 3 h with a continuous stirring until a gel was achieved. To remove residual ethanol, the gel was dried at 100 °C for 24 h. Thereafter, the powder was calcined in an oven at different temperatures (550–850 °C) for 6 h with a heating rate of 5 °C min^{-1}.

2.2 Powder Characterization

Several techniques were used for characterization of the perovskites. The thermal decomposition process of the precursor powder was carried out by thermogravimetric and differential thermal analysis TG/DTA using a SETARAM LABSYS evo at a heating rate of 10 °C.min^{-1} in air. The eventual presence of organic material after calcination was determined by infrared spectroscopy in an (FT-IR) SHIMADZU 8400 S spectrometer using KBr pellets. The phase identification of the synthesized powders, which were calcined at various temperatures, was performed from a X-ray diffraction (XRD, BRUKER-D8) by scanning the angular range 10°–80° using CuK_α radiation. The identification of crystalline phases was performed using data from the cards of JCPDS (International Center for Diffraction Data). The lattice parameters of the structure were determined by refinement of the peak positions of the XRD pattern using the program CELREF. Morphological aspects of the powders were examined by using a ESEM–FEI scanning Electron microscopy (model Quanta 600 FEG).The ultraviolet and visible diffuse reflect spectra were measured at 200–850nm wavelengths with a Perkin–Elmer–Lambda 950 spectrophotometer. The electrochemical experiments for O_2 evolution reaction were performed using a potentiostat/galvanostat instrument model Parstat 4000 and were carried out using three electrodes. Electrodes of oxides $LaNi_{1-x}Co_xO_3$ were obtained by painting on nickel support. Pt and Hg/HgO were used as auxiliary and reference electrodes, respectively.

3 Results and Discussion

3.1 TG/DTA Analysis

To further study the details in the whole chemical reaction process, the DTA–TG curves heating from 25 to 900 °C for $LaNi_{0.6}Co_{0.4}O_3$ is shown in Fig. 1. The whole process of weight loss can be divided into four stages: (1) 51–145 °C, (2) 208–311 °C, (3) 311–436 °C, (4) 744–820 °C. At the first stage of weight loss, which is correlated with a strong DTA endothermic peak at about 126 °C representing the evaporation of water and organic compounds in the gel [21]. The second stage of weight loss can be explained by the transformation of the citrate to aconitate which is accompanied by a broad endothermic peak around 239 °C [22, 23]. The third step between 311 and 436 °C, two small endothermic peaks detected on the DTA curve are centered at 344 and 399 °C. They can be probably attributed to some

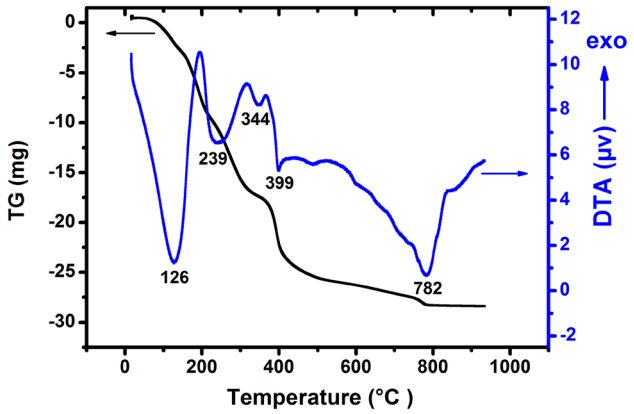

Fig. 1 TG and DTA curves of $LaNi_{0.6}Co_{0.4}O_3$ precursor heated in air at 10 °C min^{-1}

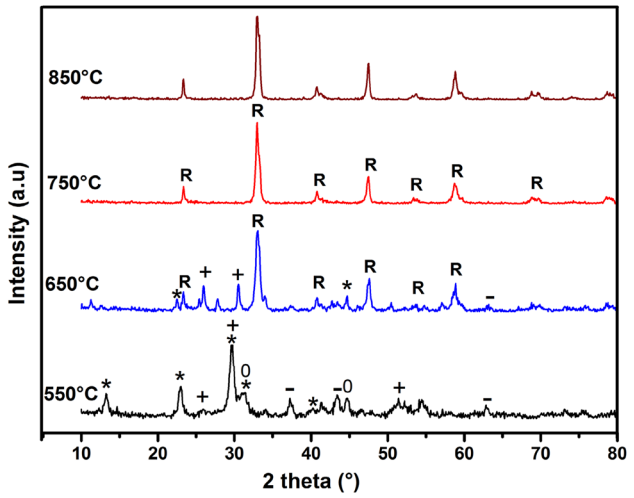

Fig. 2 XRD patterns of the $LaNi_{0.6}Co_{0.4}O_3$ powder calcined at different temperatures: (*) $La_5O_7NO_3$; (+) La_2O_3, (−) NiO; (0) Co_3O_4; (R) rhombohedral phase

chemical reactions of the organic–metal complexes with emitting some gas species like CO_2 [21]. The last endothermic peak at about 782 °C, can be possibly assigned to the gradual formation of $LaNi_{0.6}Co_{0.4}O_3$ crystal.

3.2 X-ray Diffraction

The XRD diffractograms of $LaNi_{0.6}Co_{0.4}O_3$ oxide calcined at different temperatures (550–850 °C) are presented in Fig. 2. After calcination at 550 °C, the precursor is a mixture containing $La_5O_7NO_3$ (PDF:00-038-0891), La_2O_3 (JCPDS: 01-074-1144), Co_3O_4 (JCPDS: 00-42-1467) and NiO (JCPDS: 01-089-3080). At 650 °C, the characteristic diffraction peaks of $La_5O_7NO_3$ and NiO become weaker while those of Co_3O_4 disappear. The intensity of La_2O_3 peaks becomes relatively more intense whereas the

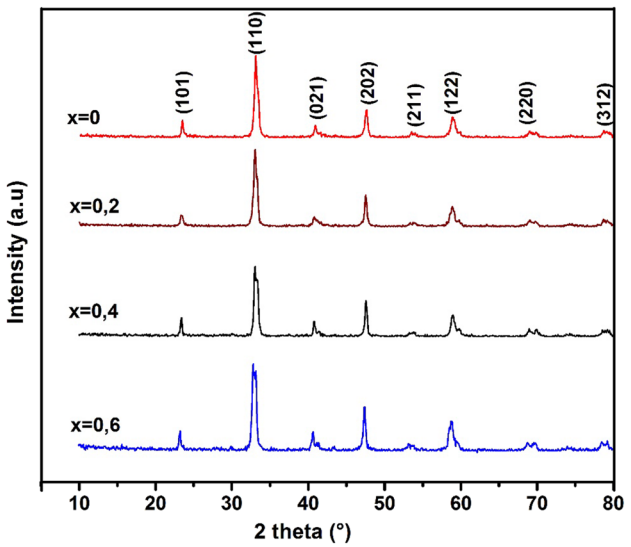

Fig. 3 X-ray diffraction patterns of perovskite $LaNi_{1-x}Co_xO_3$ ($0 \le x \le 0.6$) samples calcined at 750 °C

Table 1 Values of unit cell parameters for $LaNi_{1-x}Co_xO_3$

Nominal compositions	a = b (Å)	c (Å)	V (Å^3)
$LaNiO_3$	5.4360	6.5502	167.63
$LaNi_{0.8}Co_{0.2}O_3$	5.4293	6.5136	166.28
$LaNi_{0.6}Co_{0.4}O_3$	5.4314	6.5435	167.17
$LaNi_{0.4}Co_{0.6}O_3$	5.4481	6.5667	168.80

characteristic peaks of the rhombohedral phase appear. With the increase of calcination temperature, the peaks attributed to $La_5O_7NO_3$, La_2O_3 and NiO disappear totally at 750 °C, where the crystallinity of the $LaNi_{0.6}Co_{0.4}O_3$ phase is improved. After further heating at 850 °C, the diffractogram presents a single perovskite phase without secondary phases. The difference in the crystallization temperature of $LaNi_{0.6}Co_{0.4}O_3$ as observed in DTA and XRD could be to the difference in heating program of the samples.

XRD patterns of the $LaNi_{1-x}Co_xO_3$ ($0 \le x \le 0.6$) calcined at 750 °C for 6 h in air (Fig. 3) indicated the formation of a crystalline phase of perovskite type with rhombohedric structure (PDF: 00-034-1181). There is no distinguishable difference between the XRD patterns of $LaNiO_3$ and $LaNi_{1-x}Co_xO_3$.

The Lattice parameters a, b and c and the unit cell volume V as a function of cobalt content (x) are summarized in (Table 1). We observe that the both parameter decrease slightly with increasing x from 0 to 0.6. This is due to the incorporation of cobalt ions with bigger ionic radius (0.078 nm) in comparison with the smaller nickel ion (0.069 nm) [24]. Similar tendency has been found already for $LaNi_{1-x}Co_xO_3$ samples [16, 18, 25]. A linear variation

with respect to the substitution degree confirming the solid solution formation.

3.3 IR Spectroscopy

The sample $LaNi_{0.6}Co_{0.4}O_3$ is characterized by IR spectra in the range 400–2000 cm^{-1} (Fig. 4). From the spectra of the sample heated at 550 °C, several bands were observed with central point at 676, 800, 925, 1400 and 1596 cm^{-1}. The band observed at 676 cm^{-1} can probably be attributed to the stretching deformation of O–Ni–O [26], which becomes more strong at higher temperature. The bands which appear at about 800 and 925 cm^{-1} characterize probably the carbonate [27] and nitrate anions [28], respectively. After heating (T > 500 °C), the intensity of these bands decreases and they become less visible at higher temperature (T = 850 °C). The bands observed at 1400 cm^{-1} were assigned to stretching vibrations of carbonate [29]. This last has weakened with increasing calcination temperature. Moreover, the band at 1596 cm^{-1} corresponds to the asymmetric and symmetric carbonyl group stretching vibrations of ionized carboxylate [30]. It decreases rapidly in the temperature range 650–850 °C. The decrease in the characteristic bands of the carboxylic group and nitrate anions in the IR spectra of as burnt powder shows that ions of carboxylic group and NO_3^- take part in the reaction during combustion. Consequently, it can be considered as a thermally induced anionic redox reaction of the anionic gel wherein the carboxylic group acts as oxidant and nitrate ions act as reducers [31]. A weak band appears at ~468 cm^{-1} at 750 °C and becomes much visible at 850 °C, which corresponds to the vibration of the Ni–O bond [32].

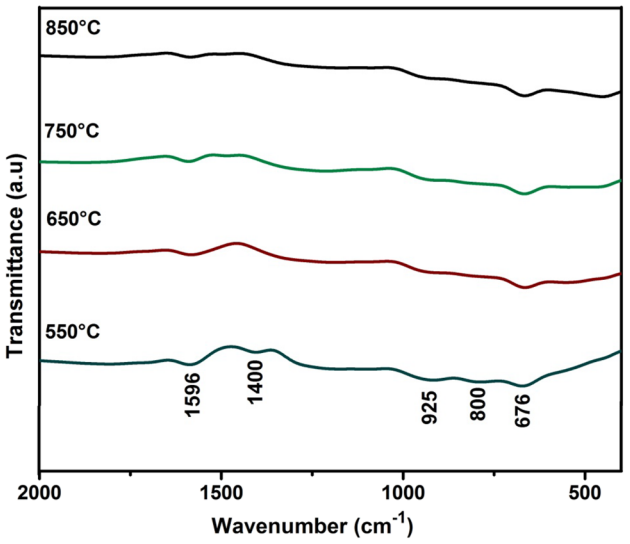

Fig. 4 Infrared spectra of $LaNi_{0.6}Co_{0.4}O_3$ powder calcined at different temperatures

Figure 5 shows the IR spectra of $LaNi_{1-x}Co_xO_3$ gels calcined at 750 °C for 6 h. All these spectra are similar in shape. Tow absorption bands located at 468 and 667 cm^{-1} can be attributed to the stretching vibration of the Ni–O bond and the stretching deformation of the O–Ni–O, respectively. They confirm the formation of perovskite structure [26, 32].

3.4 Structural and Morphological Characterization

The average crystallite size (D) was calculated from the broadening of the XRD line width by using the Debye–Scherrer relationship (Fig. 6). For that, it was necessary to consider the peaks (202) of $LaNi_{1-x}Co_xO_3$ oxides. The oxides present an average crystallite size in the range

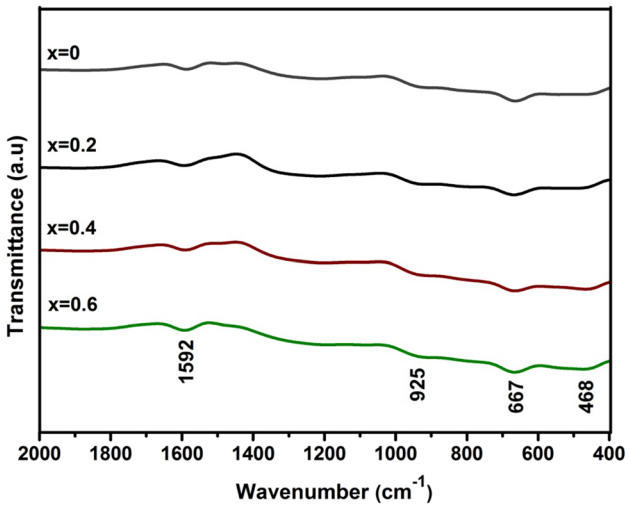

Fig. 5 Infrared spectra of $LaNi_{1-x}Co_xO_3$ ($0 \le x \le 0.6$) samples calcined at 750 °C

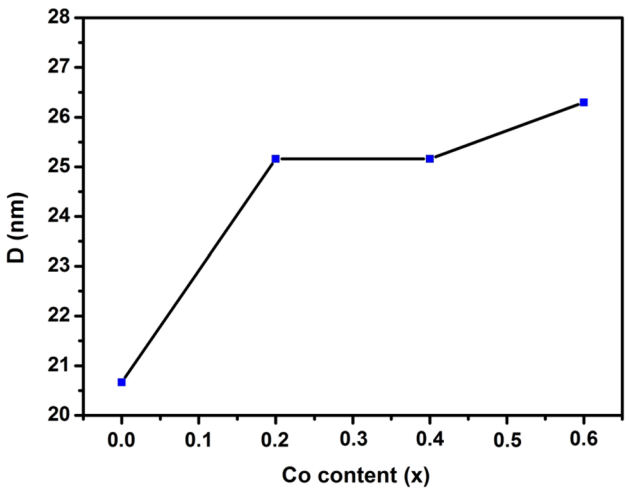

Fig. 6 Crystallite size of $LaNi_{1-x}Co_xO_3$ ($0 \le x \le 0.6$) powders

of 20.6–26.2 nm indicating that the perovskite powders prepared by the sol–gel method are composed of nanometric particles. It is observed that the crystallite size increases with increasing cobalt content. This is probably due to the incorporation of Co^{2+} into the $LaNiO_3$ lattice, which leads to the crystallite growth. Moreover, Similar results were also found previously for $LaNi_{1-x}Co_xO_3$ samples synthesized by co-precipitation method [19], $LaNi_{1-x}Co_xO_3$ [25] prepared by microwave -assisted citrate method and $LaCr_{1-x}Zn_xO_3$ ($x=0-0.3$) [33].

The morphologies of $LaNi_{1-x}Co_xO_3$($x=0-0.6$) samples studied by SEM are shown in (Fig. 7). The micrographs images indicate that particles of different shapes and sizes are formed with very well pronounced agglomeration for doped samples ($x>0.2$). The perovskites $LaNiO_3$ and $LaNi_{0.8}Co_{0.2}O_3$ are composed of almost parallelepiped grains, while samples with higher cobalt content ($x>0.2$) various shapes of grains are observed. The increase in the fraction of the doped-Co leads to highly agglomeration of particles while the porosity decreases. Similar trend of changing in size and shape were also found previously [25, 34, 35]. Indeed, it was reported that the increasing amount of cobalt in substituted calcium hydroxyapatite (HAp) increases the tendency of crystallites to stick together, leading to the formation of large particles (aggregates).

3.5 Cyclic Voltammetry

Cyclic voltammograms were registered for the electrodes $LaNi_{1-x}Co_xO_3$ calcined at 750 °C in 1 M KOH at 25 °C, the potential range $0 \le E \le 0.8$ V with the scan rate of 20 mV s^{-1}. Figure 8 shows the anodic current–potential curves of air electrode with different substitutions of cobalt content. We observe in general that these electrodes have a qualitatively similar behavior. The coated electrode films showed a good cohesion through polarization. All

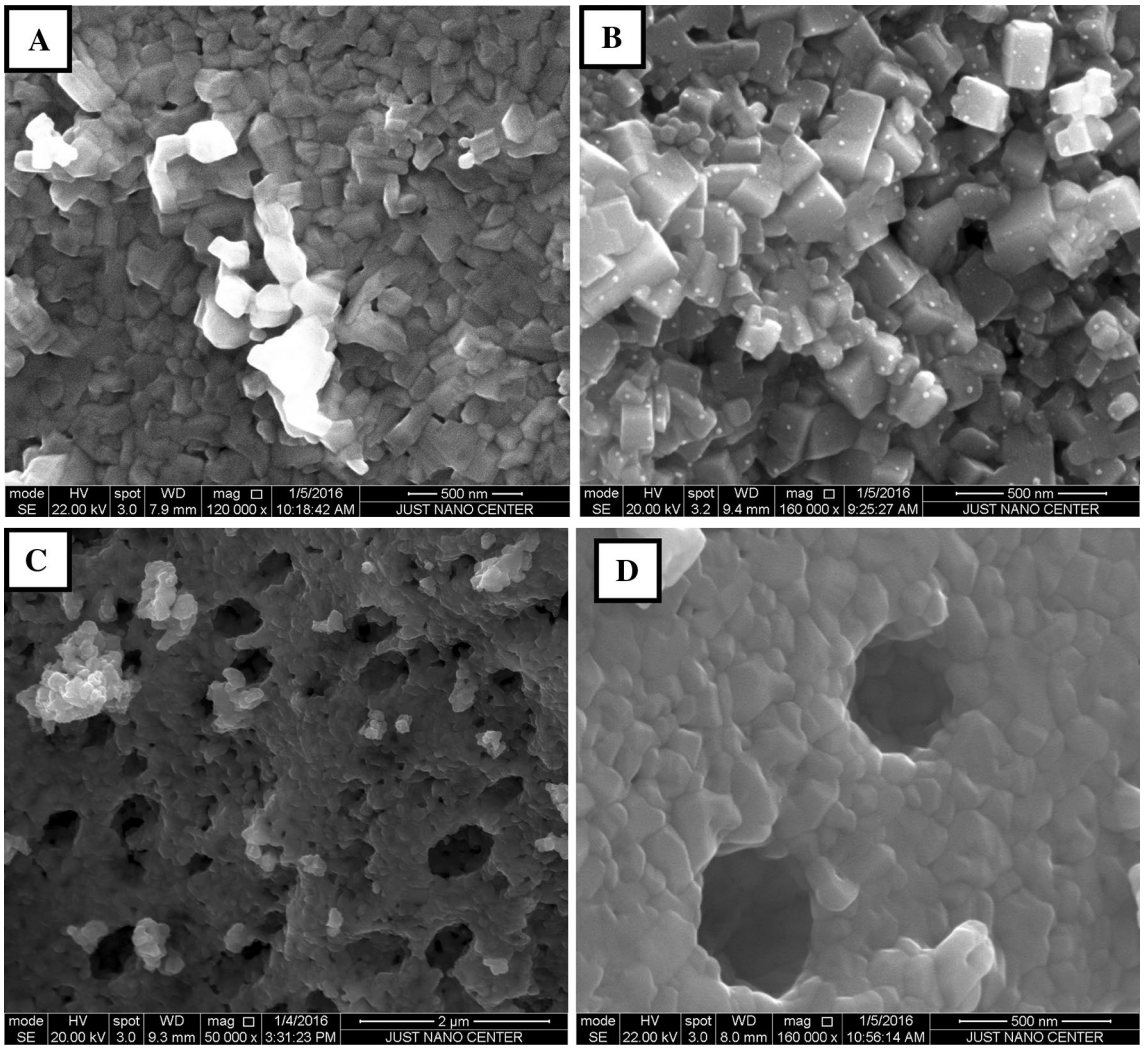

Fig. 7 SEM micrographs of $LaNi_{1-x}Co_xO_3$. **a** $x=0$; **b** $x=0.2$; **c** $x=0.4$; **d** $x=0.6$ calcined at 750 °C

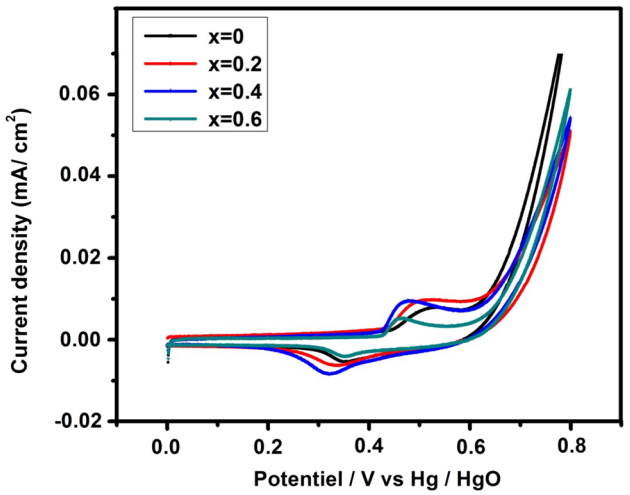

Fig. 8 The i-E polarization curves for $LaNi_{1-x}Co_xO_3$ electrodes in 1 M KOH

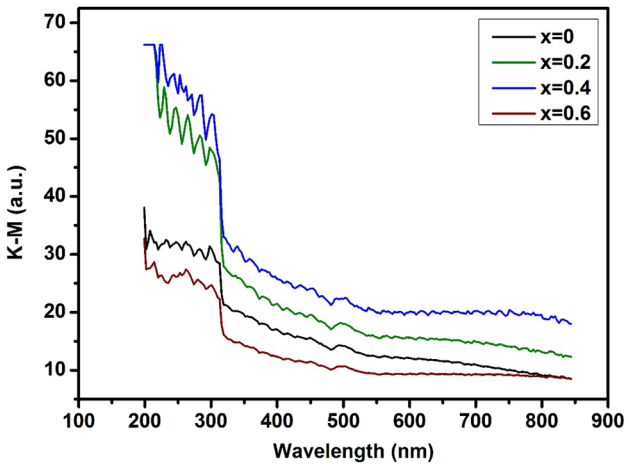

Fig. 9 Kubelka–Munk conversion spectra of the samples $LaNi_{1-x}Co_xO_3$ calcined at 750 °C

voltammograms exhibit two redox peaks. The first anodic ($470.10 \leq Epa \leq 514.27$ mV) is observed in the forward scan followed by the oxygen evolution reaction. The second one ($327.26 \leq Epc \leq 360.53$ mV) is observed in the reverse scan. These last correspond to a pseudo capacitance of the Ni(III)/Ni(II) surface redox couple [36]. The electrocatalytic activity of $LaNiO_3$ was much higher than that of doped samples. This is probably due to that nickel is more active than cobalt [37]. The same trend was also found already by Sierra et al. [38]. It has been shown that the presence of cobalt leads to a decrease of the catalytic activity attributed to the Co–Ni alloy formation. Furthermore for samples doped with cobalt, $LaNi_{0.6}Co_{0.4}O_3$ shows the high catalytic activity. This is possibly due to the porosity structure, which acts positively on the catalytic activity by increasing the number of reactant accessible catalyst sites [39].

3.6 Band Gap Study by UV–Visible Spectroscopy

The effect of doping on the energy band-gap was investigated by UV–Vis absorption spectroscopy. Figure 9 shows the Kubelka–Munk conversion spectra of as-prepared $LaNi_{1-x}Co_xO_3$ nanoparticles in the reflectance range of 200–850nm. The range of 300–570 nm is related to the metal and metal transition [40]. These spectra show that samples have similar behavior. The optical band-gap values were found to be 3.802, 3.825, 3.826 and 3.820 eV for x = 0, 0.2, 0.4, 0.6, respectively. They are higher than 3 eV, which confirms that the perovskite compounds are semiconducting in nature. The values of E_g are ranging from 0 to 5 eV, therefore the optical absorption spectra of these materials are owing probably to the highest intraband electronic transitions related to O2p and La 5d states [41]. These results indicate that the as–prepared $LaNiO_3$ and Co-doped $LaNiO_3$ nanopowders can be utilized for the photocatalysis in the degradation process of organic pollutants [42].

4 Conclusion

Co-doped $LaNiO_3$ nanopowders in the composition range x = 0–0.6 were successfully prepared via sol–gel method, employing nitrate salts of lanthanum, nickel and cobalt as cations precursors, citric acid as a chelating agent. TG-DTA curves show the thermochemical behavior of the compounds with respect to temperature. According XRD characterization, the formation of the perovskite pure phase was obtained at 750 °C with no detectable secondary phase, as well confirmed by IR spectroscopy. The morphology of samples that were examined by SEM shows that different shapes and sizes of particles are formed with very well pronounced agglomeration for doped samples (x > 0.2). In electrochemical study, $LaNi_{0.6}Co_{0.4}O_3$ electrode exhibits a significantly higher catalytic activity, indicating that this material is the best electrocatalyst for oxygen evolution reactions. The UV reflectance spectra indicate that the optical band gap values of $LaNi_{1-x}Co_xO_3$ nanoparticles are above 3 eV. This finding in optical properties indicates the potential for these doped materials to be employed in photocatalytic applications.

References

1. H. Tanaka, M. Misono, Curr. Opin. Solid State Mater. Sci. **5**, 381 (2001)

2. N. Yamazoe, Y. Teraoka, Catal. Today **8**, 175 (1990)
3. A.Y. Dobin, K.R. Nikolaev, I.N. Krivorotov, R.M. Wentzcovitch, E.D. Dahlberg, A.M. Goldman, Phys. Rev. B **68**, 113408 (2003)
4. T. Aytug, B.W. Kang, C. Cantoni, E.D. Specht, M. Paranthaman, A. Goyal, D.K. Christen, D.T. Verebelyi, J.Z. Wu, R.E. Ericson, C.L. Thomas, C.Y. Yang, S.E. Babcock, J. Mater. Res. Bull. **16**, 2661 (2001)
5. G. Catalan, R.M. Bowman, J.M. Gregg, Phys. Rev. B **62**, 7892 (2000)
6. E. Pietri, A. Barrios, O. Gonzalez, M.R. Goldwasser, M.J. Pérez-Zurita, M.L. Cubeiro, J. Goldwasser, L. Leclercq, G. Leclercq, L. Gingembre, Stud. Surf. Sci. Catal. **136**, 381 (2001)
7. F.T. Akin, J.Y.S. Lin, J. Memb. Sci. **231**, 133 (2004)
8. E. Campagnoli, A. Tavares, L. Fabbrini, I. Rossetti, Y.A. Dubitsky, A. Zaopo, L. Forni, Appl. Catal. B **55**, 133 (2005)
9. S. Liu, X. Tan, K. Li, R. Hughes, Ceram. Int. **28**, 327 (2002)
10. A.A. Leontiou, A.K. Ladavos, P.J. Pomonis, Appl. Catal. A **241**, 133 (2003)
11. K. Kleveland, M.-A. Einarsrud, T. Grande, J. Eur. Ceram. Soc. **20**, 185 (2000)
12. M. Nazari, N. Ghasemi, H. Maddah, M.M. Motlagh, J. Nanostruct. Chem. **4**, 1 (2014)
13. E.L. Crepaldi, P.C. Pavan, J.B. Valim, J. Braz, Chem. Soc. **11**, 64 (2000)
14. L.P. Rivas-Vazquez, J.C. Rendon-Angeles, J.L. Rodriguez-Galicia, K. Zhu, K. Yanagisawa, Solid State Ion **172**, 389 (2004)
15. P. Shikha, T.S. Kang, B.S. Randhawa, J. Alloys Compd. **625**, 336 (2015)
16. G. Valderrama, A. Kiennemann, M.R. Goldwasser, Catal. Today **133**, 142 (2008)
17. J. Androulakis, J. Giapintzakis, Phys. B **405**, 107 (2010)
18. C.R.B. Silva, L. da Conceição, N.F.P. Ribeiro, M.M.V.M. Souza, Catal. Commun. **12**, 665 (2011)
19. S. Zhong, Y. Sun, H. Xin, C. Yang, L. Chen, X. Li, Chem. Eng. J. **275**, 351 (2015)
20. L. Zhao, T. Han, H. Wang, L. Zhang, Y. Liu, Appl. Catal. B **187**, 19 (2016)
21. M. Liu, D. Xue, C. Luo, J. Alloys Compd. **426**, 118 (2006)
22. Y.-M. Hon, K.-Z. Fung, M.-H. Hon, J. Eur. Ceram. Soc. **21**, 515 (2001)
23. R. Alcantara, P. Lavela, J.L. Tirado, R. Stoyanova, E. Kuzmanova, E. Zhecheva, Chem. Mater. **9**, 2145 (1997)
24. S. Makhloufi, M. Omari, J. Inorg. Organomet. Polym. Mater. **26**, 32 (2016)
25. A. Galal, N.F. Atta, S.M. Ali, Electrochim. Acta **56**, 5722 (2011)
26. A. Wokaun, B. Schrader, *Infrared and Raman Spectroscopy-Methods and Applications*. (VCH, Weinheim, 1995)
27. J.M.D. Tascón, L.G. Tejuca, J. Chem. Soc. Faraday Trans. 1 **77**, 591 (1981)
28. A. Mali, A. Ataie, Scr. Mater. **53**, 1065 (2005)
29. M. Hadioui, Doctoral Thesis, University of Toulouse, 2007
30. P. Tarte, Spectrochim. Acta Part A **23**, 2127 (1967)
31. K. Adaika, M. Omari, J. Sol–Gel Sci. Technol. **75**, 298 (2015)
32. A. Leleckaite, A. Kareiva, Opt. Mater. **26**, 123 (2004)
33. I. Chadli, M. Omari, M. A. Dalo, B. A. Albiss, J. Sol–Gel Sci. Technol. **80**, 598 (2016)
34. B. Babu, C.V. Reddy, J. Shim, R. Ravikumar, J. Park, J. Mater. Sci. **27**, 5197 (2016)
35. Z. Stojanović, L. Veselinović, S. Marković, N. Ignjatović, D. Uskoković, Mater. Manuf. Process **24**, 1096 (2009)
36. M. Lebid, M. Omari, Arab. J. Sci Eng. (2014)
37. M.C.J. Bradford, M.A. Vannice, Catal. Rev. **41**, 1 (1999)
38. G.S. Gallego, C. Batiot-Dupeyrat, J. Barrault, E. Florez, F. Mondragón, Appl. Catal. A **334**, 251 (2008)
39. A.R. Oveisi, K. Zhang, A. Khorramabadi-Zad, O.K. Farha, J.T. Hupp, Sci. Rep. **5**, (2015)
40. T. Wang, T. Xu, S. Gao, S.-H. Song, Ceram. Int. **43**, 4489 (2017)
41. L. Guan, B. Liu, L. Jin, J. Guo, Q. Zhao, Y. Wang, G. Fu, Solid State Commun. **150**, 2011 (2010)
42. A. Hernández-Ramirez, I. Medina-Ramirez, *Photocatalytic Semiconductors: Synthesis, Characterization, and Environmental Applications* (Springer, New york, 2014)